no significant streamwise variation in GV wavelength occurred for any of the three freestream velocities.

Conclusions

Spanwise varying velocity components within GVs were obtained with a three-dimensional LDA. The w disturbance was only detectable near the wall ($y/\delta = 0.143$), whereas the u and v disturbances were detectable higher up in the boundary layer ($y/\delta = 0.429$). The data were well correlated with sinusoidal variations, and the estimated vortex wavelength from these measurements matched theoretical expectations. Measurements taken at other freestream velocities and x locations indicated streamwise conservation of GV wavelength.

References

[1]Görtler, H., "On the Three-Dimensional Instability of Laminar Boundary Layers on Concave Walls," NACA TM 1375, June 1954 (English translation).

[2]McCormack, P. D., Welker, H., and Kelleher, M., "Taylor-Goertler Vortices and Their Effect on Heat Transfer," *Journal of Heat Transfer*, Vol. 102, No. 1, 1970, pp. 101–112.

[3]Winoto, S. H., Durão, D. F. G., and Crane, R. I., "Measurements Within Görtler Vortices," *Journal of Fluids Engineering*, Vol. 101, 1979, pp. 517–520.

[4]Floryan, J. M., "On the Görtler Instability of Boundary Layers," National Aerospace Lab., TR-1120T, Tokyo, Japan, Aug. 1991.

[5]White, F. M., *Viscous Fluid Flow*, 2nd ed., McGraw–Hill, New York, 1991, p. 368.

Navier–Stokes Simulation of a Cone-Derived Waverider with Multidirectional Curvature

Sheam-Chyun Lin* and Ming-Chiou Shen†
National Taiwan Institute of Technology, Taipei, Taiwan 10772, Republic of China

Introduction

THE idea of using a waverider concept as the primary basis of designing a hypersonic vehicle has been considered seriously in the last decade. In 1980, Rasmussen[1] derived waveriders from the circular and elliptic cones by the perturbation method on the basis of hypersonic small-disturbance theory (HSDT), and then Rasmussen et al.[2] conducted an experiment proving that this analytic approximation is highly credible. Later, Lin and Rasmussen[3] extended the circular cone solution to include the transverse and longitudinal curvatures. Consequently, the waverider shapes with multidirectional curvature (MDCWR)[4] are created by using this solution. It was shown that the MDCWR has the advantage of efficient volumetric packaging and enhanced lift-to-drag ratio (L/D).

Recently, Liao et al.[5] simulated the flowfields for the elliptic-cone-derived waverider (ECDWR) of Rasmussen et al.[2] at both design and off-design flight conditions. They found that the shock wave still did not attach to the wing tip under the on-design conditions. Also, an obvious vortex occurred on the upper surface when the angle of attack increased to 5 deg. Until now, no numerical simulation for the MDCWR has been performed systematically. Therefore, the numerical simulation for the MDCWR is studied in this work. The analysis investigates both on-design Mach 4 and off-design conditions, including angles of attack from 0 to 10 deg and Mach numbers from 2 to 6. In addition, these numerical results are compared with the previous studies of the ECDWR.[5]

Received Nov. 1, 1995; presented as Paper 96-0313 at the AIAA 34th Aerospace Sciences Meeting, Reno, NV, Jan. 15–19, 1996; revision received April 1, 1996; accepted for publication April 7, 1996.

*Associate Professor, Department of Mechanical Engineering. Member AIAA.

†Graduate Research Assistant, Department of Mechanical Engineering.

Waverider Generation and Numerical Method

In this Note, a fourth-order freestream trailing-edge curve with zero-slope edge with the approximate analytic solution of Lin and Rasmussen[3] and Lin and Luo[4] is selected to generate the MDCWR. For comparison with previous investigations of the ECDWR, all design parameters and flight conditions except the longitudinal curvature are identical to those of the ECDWR reported by Rasmussen et al.[2] and Liao et al.[5] Also, the flow was considered laminar. Moreover, the inability to estimate viscous effect in HSDT is compensated by using an average skin-friction coefficient ($\bar{C}_f$), proposed by He and Rasmussen,[6] for comparing with the viscous numerical results.

The three-dimensional compressible Navier–Stokes equations are solved by using Roe's implicit, finite volume, upwind algorithm.[7] By means of the monotone upstream-centered schemes for conservation laws interpolation of the primitive variables, the quantity in the inviscid fluxes is obtained. Furthermore, the thin-layer approximation is utilized for each viscous direction to calculate the viscous flux terms by a second-order central difference. Moreover, the impermeable and adiabatic wall boundary conditions are imposed in the present calculations. The outer boundary and initial flow conditions are specified as freestream flow properties. In addition, a calorically perfect gas was assumed here. With regard to the grid generation, a Poisson's equation,[8] together with a nonlinear successive over-relaxation technique, is used to generate a full three-dimensional boundary-fitted grid in the convergence criterion that the maximum error for each iteration is less than 10^{-5}. Here, two grid systems of $51 \times 106 \times 81$ (see Fig. 1) and $26 \times 54 \times 40$, which clustered near the shock layer, wall, apex, and wing tip of the MDCWR, are generated to test the grid independence.

Results and Discussion

Before proceeding with the investigation of the waverider, two model problems are considered to validate the present numerical techniques, results of which are summarized in Table 1. The solutions of these model problems confirm that the numerical procedure does perform as expected.

Table 1 Model problems

Case	$Re \times 10^6$	M_∞	Grid size	Comparison	Error, %
Flat plate	1.0	4.0	101×101	Van Driest[9]	0.12
ECDWR	3.94	4.0	$41 \times 91 \times 51$	Liao et al.[5]	0.62

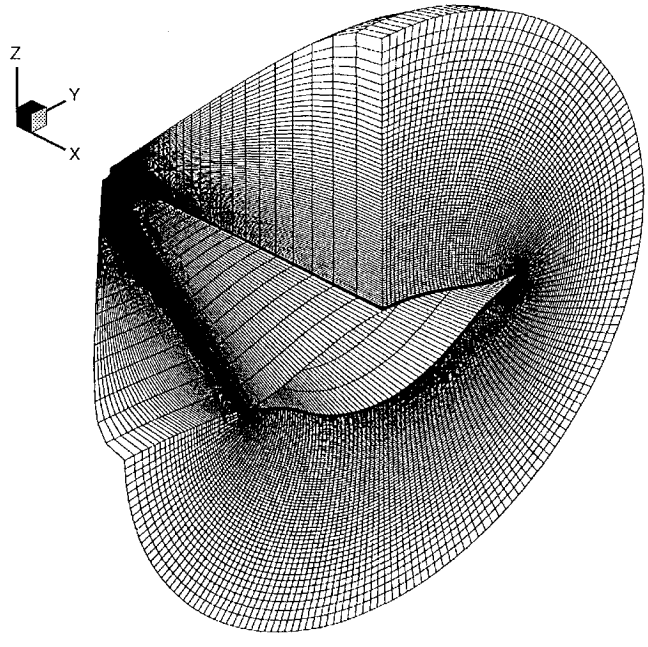

Fig. 1 Three-dimensional grid for MDCWR ($51 \times 106 \times 81$).

Table 2 Comparisons at on-design conditions

	Inviscid			Viscous		
Type	Euler	HSDT	Error, %	Navier–Stokes	HSDT	Error, %
C_L	0.7850	0.8095	3.0	0.7806	0.8095	3.6
C_D	0.2156	0.2269	5.0	0.2245	0.2341	4.1
$\bar{C}_f \times 10^2$	0	0	0	0.7220	0.7627	5.3
L/D	3.6410	3.5677	2.1	3.4771	3.4579	0.6

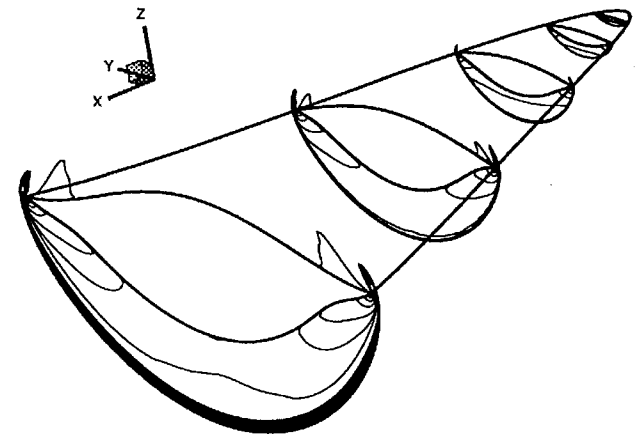

a) At several cross sections

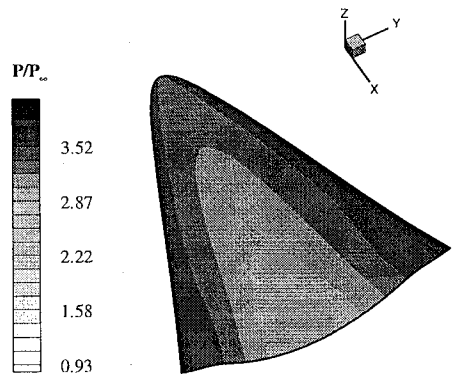

b) On the lower surface

Fig. 2 On-design pressure contours (M_∞ = 4.0 and α = 0 deg).

In this research, each case was performed on the DEC 3600 workstation with 64 megabytes of memory, and the computational efficiencies are 1.14×10^{-4} CPU s/grid/iteration. The L_2 residuals can be dropped 4–5 orders to reach 10^{-9} after about 3500 iteration time steps, which correspond to a total CPU time of about 50–55 h. The results show that the grid numbers within the boundary layer for the fine and coarse grid systems are 19 and 11 points, respectively. Also, the difference of $\bar{C}_f$ for these grid systems is only 3%. To adapt the wide flight conditions, the fine grid is thus chosen here.

For on-design conditions, freestream Mach number of 4, and 3.94×10^6 for the Reynolds number base on the waverider length, Fig. 2a illustrates the pressure contours at several cross planes along the entire body. Similar to the existing numerical results for waveriders,[5,6] the shock is slightly away from the wing tip because of the approximate nature of the HSDT and the numerical method. Figure 2b plots the computed pressure contours on the lower surface. As expected from theoretical prediction,[3] the pressure exhibits an increasing trend in the span direction because of the transverse curvature, and owing to the longitudinal curvature, a Prandtl–Meyer expansion occurs and the pressure decreases as the flow moves downstream.

The on-design aerodynamic properties calculated by both the numerical method and HSDT are listed in Table 2. Note that the base drag is ignored, and the base area was used as reference area for calculating force coefficients. It is obvious that all of the values of the flowfields predicted from the HSDT correlate well with the numerical results. Similar to the ECDWR's results,[5] the lift coefficients for viscous and inviscid cases are almost identical because the viscous effects are confined to a well-behaved laminar boundary layer.

Table 3 Off-design aerodynamic properties

M_∞	α, deg	C_L	C_D	$\bar{C}_f \times 10^2$	L/D	Δz_{sm}
2.0	0	1.0546	0.2720	0.9404	3.8877	−0.1224
3.0	0	0.8744	0.2410	0.7851	3.6282	−0.1191
4.0	0	0.7806	0.2245	0.7220	3.4771	−0.1176
4.0	5	1.2530	0.4363	0.6973	2.8719	−0.1201
4.0	10	1.6941	0.7505	0.7170	2.2573	−0.1213
5.0	0	0.7269	0.2139	0.6819	3.3983	−0.1166
6.0	0	0.6931	0.2059	0.6587	3.3662	−0.1153

Table 4 Comparisons between MDCWR and ECDWR

	$M_\infty = 4, \alpha = 0$ deg		$M_\infty = 4, \alpha = 5$ deg	
Type	ECDWR	MDCWR	ECDWR	MDCWR
C_L	0.7632	0.7806	1.1906	1.2530
C_D	0.2347	0.2245	0.4404	0.4363
$\bar{C}_f \times 10^2$	0.7370	0.7220	0.6720	0.6973
L/D	3.2515	3.4771	2.7037	2.8719
$V^{2/3}/S_p$	0.1904	0.2713	—	—

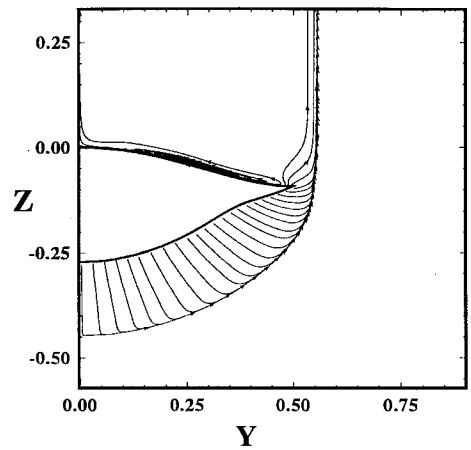

Fig. 3 Off-design particle traces in the base plane (M_∞ = 4.0 and α = 5 deg).

As the angle of attack increases to 5 deg, Fig. 3 reveals that a vortex is generated on the upper surface. However, the vortex for the present waverider is much more slender and smaller than that which was observed with previous ECDWR.[5] Table 3 lists the computed force coefficients, L/D, and static margin (Δz_{sm}) for various flight conditions. Obviously, the lift and drag coefficients increase monotonically with the increase of the angle of attack. In contrast, the L/D decreases with the increase of the angle of attack in a linear relation as $(L/D)_\alpha = (L/D)_{\alpha=0} \times (1 - 0.035\alpha)$. In addition, the aerodynamic performances decrease monotonically except for the static margin with the increase of flight Mach numbers. However, the maximum decrement of L/D between design and off-design Mach numbers is less than 3.5%. As the flight condition alters, the variation of the static margin that is calculated based on the assumption of a homogeneous body is slight.

Finally, the comparison between MDCWR and ECDWR is tabulated in Table 4. It is evident that the trends of aerodynamic performances for MDCWR are similar to ECDWR under different flight conditions. However, a superior performance and volumetric ratio (volume$^{2/3}$/planform area) are also observed for MDCWR.

Conclusions

A comprehensive three-dimensional, laminar flowfield simulation of MDCWR has been performed. The analysis studies both inviscid and viscous on-design Mach 4 and viscous off-design conditions, including angles of attack from 0 to 10 deg and Mach numbers from 2 to 6. Under on-design conditions, it is found that both the inviscid and viscous numerical simulations are in good correlation with the HSDT's prediction; thus the reliability and accuracy

of the analytical approximate solution are examined and validated for the MDCWR. In addition, under the off-design conditions, the decreases in L/D and static margin are slight even though the angle of attack and Mach number alter. Moreover, after comparing the ECDWR with the present waverider, the advantage of longitudinal curvature is verified by an increased volumetric ratio, enhanced L/D, and wider range of flight conditions than ECDWR. Notably, the viscous drag will increase considerably, as a percentage of the total drag, as the generating angle for the waverider decreases and as the flight conditions result in turbulent flow.

Acknowledgment

The authors would like to thank the National Science Council of the Republic of China for financial support of this manuscript under Contract 83-0424-E-011-050.

References

[1]Rasmussen, M. L., "Waverider Configurations Derived from Inclined Circular and Elliptic Cones," *Journal of Spacecraft and Rockets*, Vol. 17, No. 6, 1980, pp. 537–545.

[2]Rasmussen, M. L., Jischke, M. C., and Daniel, D. C., "Experimental Surface Pressure on Cone-Derived Waveriders for $M = 3-5$," *Journal of Spacecraft and Rockets*, Vol. 20, No. 6, 1983, pp. 539–545.

[3]Lin, S. C., and Rasmussen, M. L., "Cone-Derived Waverider with Combined Transverse and Longitudinal Curvature," AIAA Paper 88-0371, Jan. 1988.

[4]Lin, S. C., and Luo, Y. S., "Integrated Inlets for Cone-Derived Waverider with Combined Transverse and Longitudinal Curvature," *Journal of Spacecraft and Rockets*, Vol. 31, No. 4, 1994, pp. 609–614.

[5]Liao, J. R., Isacc, K. M., Miles, J. B., and Tsai, B. J., "Navier–Stokes Simulation for Cone-Derived Waverider," *AIAA Journal*, Vol. 30, No. 6, 1992, pp. 1521–1528.

[6]He, X., and Rasmussen, M. L., "Computational Analysis of Off-Design Waveriders," *Journal of Spacecraft and Rockets*, Vol. 31, No. 2, 1994, pp. 345–353.

[7]Roe, P. L., "Approximate Riemann Solvers, Parameter Vectors and Difference Schemes," *Journal of Computational Physics*, Vol. 43, No. 2, 1981, pp. 357–372.

[8]Thompson, J. F., and Warsi, Z. U. A., "Boundary-Fitted Coordinate Systems for Numerical Solution of Partial Differential Equations: A Review," *Journal of Computational Physics*, Vol. 47, No. 1, 1982, pp. 101–108.

[9]Van Driest, E. R., "Investigation of Laminar Boundary Layer in Compressible Fluids Using the Crocco Method," NACA TN 2579, Jan. 1952.

Momentum and Vortex Theory of Rotor Blade Wakes

Walter C. Hassenpflug*
University of Stellenbosch,
Stellenbosch 7600, South Africa

Introduction

THE customary impulse-momentum theory for a rotor disk in vertical flight establishes a relation between thrust and induced velocity in the far wake. Steady frictionless flow is assumed, and uniform ambient pressure in the far wake, corresponding to infinitely many blades. The exact flow in the wake due to a finite number of blades can be calculated using vortex theory. The customary approximation is to assume a rigid vortex sheet, which flows down with uniform wake velocity for the ideal rotor operation.

Prandtl[1,2] has used the approximation that the blade lift from momentum theory only differs substantially at the blade tips. He approximated the flow from the blade tips in the far wake by a two-dimensional flow of parallel half-infinite vortex sheets. This model is a good approximation of the exact calculations of the rigid vortex model by Goldstein.[3] Goldstein's model has led Theodorsen[4] to conclude that the pressure in the far wake is higher than the surrounding atmospheric pressure, contrary to impulse-momentum theory. More recently Bramwell[5–7] has used the two-dimensional tip vortex sheet approximation of Prandtl to calculate the overpressure $(p - p_\infty)/\rho = \frac{1}{2}V_\infty^2$ in the far wake, where V_∞ is the uniform flow velocity outside upwards, relative to the vortex sheet cascade, and the surrounding atmospheric pressure is p_∞. This contradicts the assumption and conclusion of the impulse-momentum theory, albeit by a small amount. In a recent revision of Theodorsen's theory, Ribner[8] still uses this result.

However, this theory cannot be correct. Betz[9] has pointed out that horizontal finite forces at the vortex sheet tips would be required to sustain the rigid vortex sheet, and the absence of these forces is the cause for roll-up.

It will be shown subsequently that, to correct the unbalance from the rigid state, the very edge of the vortex sheet, with infinitesimal vortex strength, moves upwards with infinite velocity, therefore creating an unsteady flow with a corresponding additional pressure field. This concept was presented originally in Ref. 10.

Vortex Sheet Cascade

As approximation the two-dimensional flow over a cascade of finite width sheets is used. The potential flow is obtained by conformal mappings like those given by Kober[11] or Betz.[12] The width of the cascade is taken as 2, the right edge being at $x = 1$, and the pitch as h. The loading of the elliptic wing is approached as $h \to \infty$ with constant downwash velocity V_∞, Prandtl's tip wake flow is approached as $h \to 0$ with constant product $V_\infty h$, and uniform rectangular loading is approached as $h \to 0$ with constant V_∞.

Steady Flow

The pressure of steady flow relative to the vortex sheet from Bernoulli's equation is shown as carpet plot along lines parallel to the vortex sheets in Fig. 1 for $h = 0.5$. Practical values of h are of this order. As an example, the Westland model 30 helicopter at max takeoff weight of 12,800 lb would produce a far wake at hover with spacing of $h = 0.37$. The pressure is seen to be almost $\frac{1}{2}\rho V_\infty^2$ between the sheets except for end effects.

From Blasius' theorem for steady flow horizontal forces at the edges, $f_x = c_1 \frac{1}{2}\rho V_\infty^2$, are found, where c_1 is a constant depending on h. Although these forces would not enter the vertical balance in momentum theory, they do require the overpressure between the sheets to satisfy the horizontal equilibrium of half a vortex sheet.

Unsteady Flow

In this simplified model the unsteady flow starts when the edge forces of steady flow are removed instantaneously. Therefore all of the edge vortices of infinitely small size start suddenly with infinite

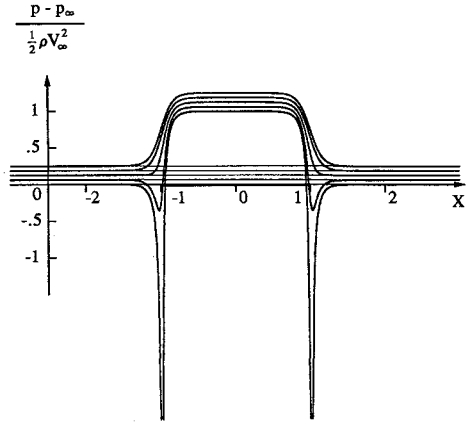

Fig. 1 Steady part of pressure of cascade, $h = 0.5$.

Received Sept. 6, 1994; revision received Sept. 20, 1995; accepted for publication Sept. 20, 1995.

*Senior Lecturer, Department of Mechanical Engineering.